Minibands in the Continuum of Multi-Quantum-Well Superlattices

D. Gershoni, J. Oiknine-Schlesinger, E. Ehrenfreund, and D. Ritter
Solid State Institute, Technion-Israel Institute of Technology, Haifa 32000, Israel

R. A. Hamm and M. B. Panish
AT&T Bell Laboratories, Murray Hill, New Jersey 07974
(Received 21 June 1993)

We report the first observation of well defined minibands and minigaps between them, at energies above the barriers in multi-quantum-well structures. Using intersubband absorption spectroscopy, we have observed the optical transitions between confined electronic states of isolated quantum wells to minibands in the continuum of the periodic structure. By comparison with a theoretical model we spectroscopically identify all the observed transitions and explain their strength and spectral shape. In addition, we estimate the coherence length of the electronic wave function in these minibands comparing the absorption spectrum with that of a finite array of quantum wells.

PACS numbers: 71.25.−s, 73.20.Dx, 73.60.Br

The low energy spectrum of a one-dimensional periodic potential is composed of energy bands separated by forbidden gaps. The bandwidth of these energy bands is a direct measure of the overlap integral between states of neighboring periods. In the limit of vanishing overlap the bandwidth vanishes and the bands become degenerate, corresponding to the extreme case in which noninteracting isolated wave functions are confined in each period. When the overlap is not negligible, the bands have a finite bandwidth, and the wave functions of states within these bands spread over the whole structure. In the opposite limit of extreme overlap, bands originating from different states merge together, the forbidden gaps disappear, and an energy continuum is formed.

A multi-quantum-well (MQW) semiconductor heterostructure is an artificial periodic potential for carriers in which both limits coexist. As the name MQW suggests, in such a structure states having an energy smaller than the barrier's potential are not different from the corresponding states of a single quantum well (QW). They are degenerate, since wave functions of different QWs do not overlap. States with an energy which is greater than the potential of the barrier, however, are different. In contrast with the continuum of an isolated QW, they form nondegenerate minibands of finite bandwidth, separated by forbidden minigaps in which the density of levels strictly vanishes. The number of minibands and minigaps below the onset of the continuum and their bandwidth depends on the details of the periodic potential structure. In addition, the miniband structure depends also on the phase coherence length of electrons in this material, since the wave functions of states in these minibands must maintain their coherence over more than one period in order for the MQW degeneracy to be removed.

Optical and transport properties of various MQW and superlattice (SL) structures have been widely studied [1–5]. In these studies, the existence of both degenerate levels and minibands is well established. Observations of a miniband in the energy range above the barrier potential have already been reported by a few groups. In particular, infrared detectors based on optical transition from a degenerate level to a continuum miniband are found to be very efficient [6]. Recently, the observation of a miniband at energy above the QW or SL barrier was reported for a special design where a Bragg reflector is used to confine carriers to the barrier's region [7]. However, there have been no reports on the observation of minigaps in this energy range. Moreover, there has never been a report on the observation of more than one miniband in the continuum, a situation which is no different from the case of a single quantum well, for which the appearance of fluctuations in the density of levels close to the barrier potential are expected.

In this Letter we report the first observation of minibands and minigaps in the continuum of a MQW structure. The miniband structure of the MQW is studied via the optical transitions from a discrete electronic level within separated QWs to collective MQW minibands in the continuum. We also show that the coherence length of carriers in these minibands can be estimated directly from the optical measurements.

The optical measurements were performed on two samples of InGaAs/InP MQW structures lattice matched to InP. The samples were grown by metalorganic molecular beam epitaxy (MOMBE) [8]. The first sample contained a background n-type doping concentration of $<1\times10^{16}$ cm^{-3} both in the ternary QWs and the binary barriers. It contained 15 periods of a 65 Å InGaAs well followed by a 367 Å InP barrier. The second was n-type doped with 5×10^{17} cm^{-3} Sn impurities within the ternary QWs only. It contained 20 periods of a 62 Å InGaAs well cladded between 569 Å InP barriers. The dimensions of the samples were determined by high resolution x-ray diffraction [9] and transmission electron microscopy [8]. The carrier concentration was estimated from Hall measurements performed on thick (>1 μm) ternary and binary layers grown under similar conditions.

In Fig. 1 we display the calculated conduction band

0031-9007/93/71(18)/2975(4)$06.00

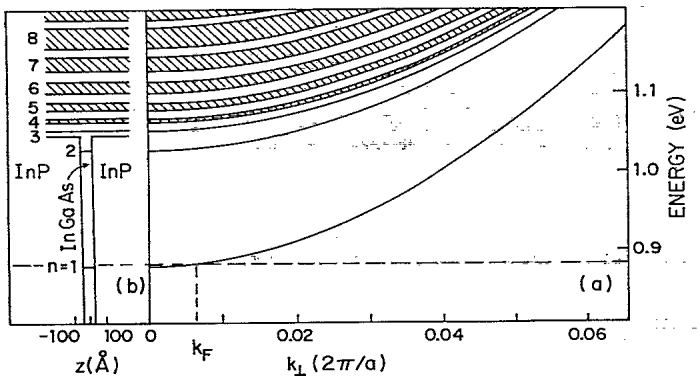

FIG. 1. (a) Calculated MQW conduction band dispersion relations for sample 1 plotted as energy vs in-plane wave vector, $k_\perp$. The electronic Fermi energy is marked as a horizontal dashed line. (b) Schematic representation of the energy subbands and potential for electrons in one period of the structure.

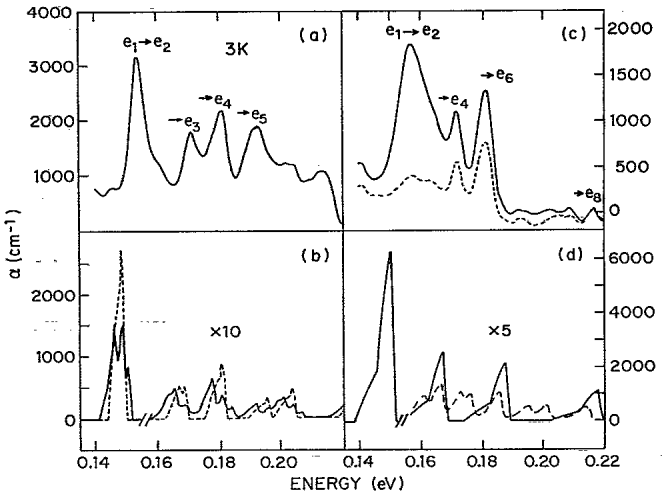

FIG. 2. Measured (a) and calculated (b) intersubband absorption for sample 1. The dashed line in (b) shows the calculated spectra for the nominal MQW dimensions and the solid line is an average over ± 1 monolayer fluctuations, keeping the same periodicity. Measured (c) and calculated using nominal MQW dimensions (d) intersubband absorption for sample 2. The solid (dashed) line in (c) is for radiation polarized parallel (perpendicular) to the MQW axis. The solid (dashed) line in (d) is for calculations with contributions from one (three) different points within the MQW BZ.

structure of the first MQW. The calculations were performed with the Baraff and Gershoni (BG) model [10] which uses expansion of the eight band envelope functions in a Fourier series in the coordinate parallel to the SL axis (the material parameters used are listed in Ref. [11]). The effect of the SL band structure, as a result of the overlap of wave functions of adjacent wells, is accommodated into the model scheme by performing the calculations at several points within the first SL Brillouin zone (BZ) [10]. This overlap manifests itself in the formation of minibands of finite energy width as shown by the shaded areas of Fig. 1. We count up to 8 minibands of increasing width, well separated by forbidden minigaps, before the onset of the MQW continuum takes place at $\simeq$150 meV above the bottom of the InP barrier conduction band energy.

The matrix elements for optical transitions between the conduction subbands are calculated using the dipole approximation [11]. It is important to note that this calculation takes into account contributions to the matrix element from both the dipole moment between the envelope wave functions and the dipole moment between the Bloch wave functions. Counterintuitively and unlike what is stated in most of the literature, following the pioneering work of West and Eglash [1], the Bloch wave function contribution is the most important one. Indeed, as first noted by Zawadzki [12], the envelope wave function contribution to the matrix elements can be completely neglected since it is smaller by roughly a factor of the electron effective mass squared than the contribution of the Bloch wave functions. Thus, it is the *a priori* introduction of the electron effective mass into the radiation-matter interaction Hamiltonian which makes the common model [13] useful. It fails, however, for the inter-sub-valence-band calculations [14], and, likewise, it does not yield reliable results for optical transitions to expanding or continuum conduction minibands, which is the subject of the present Letter.

Figure 2(a) displays the measured absorption spectrum of the first sample for unpolarized infrared (ir) radiation. For these measurements the sample was fabricated in a waveguide configuration and placed in a helium immersion cryostat. The cryostat was placed in a step-scan Fourier transform ir spectrometer. In Fig. 2(b) we display the calculated intersubband absorption spectrum of the first sample. The dashed line represents calculations with the nominal dimensions of the structure. The solid line represents an average over three different calculations for structures with the same period length and ± 1 monolayer QW thickness difference. Uniform electron density of 1×10^{16} cm^{-3} and an ambient temperature of 3 K were used for the calculations. We marked the peaks in the figures by the electronic transition between initial and final minibands, which contributes most to their oscillator strength. Note that the calculated transitions have an asymmetrical line shape, with sharper edge at higher energies. This intrinsic asymmetry, which can be viewed as resulting from the electron mass nonparabolicity, is completely washed by the broadening due to the well width fluctuations.

Comparing the measured [Fig. 2(a)] and calculated [Fig. 2(b)] spectra we see that our model describes well the energy position and the spectral shape of the observed transitions. The absolute value of the $e1$-$e2$ calculated transition agrees within less than a factor of 2 with the measured one. This is well within the error associated with the estimated density of Si dopants. The calculated intensity of the optical transitions to the continuum minibands are almost an order of magnitude smaller than the measured values. This discrepancy will be discussed

below. In addition we note the following.

(a) The lowest optical transition is the $e1$-$e2$ transition. This is a symmetry allowed optical transition between two confined electronic states within the InGaAs QW. It is about an order of magnitude stronger than the next symmetry allowed transition $e1$-$e4$, from the first confined state to a continuum miniband. The relative strength of the $e1$-$e4$ transition in our MQW is about a factor of 200 larger than the corresponding transition in an infinite QW [1]. The intensity ratio between the $e1$-$e4$ and $e1$-$e2$ transitions scales with the MQW duty cycle, or, roughly speaking, with the overlap between the confined $e1$ to the expanding state $e4$.

(b) The transitions $e1$-$e3$ and $e1$-$e5$ which are forbidden in a symmetric single QW are clearly observed in the measured and calculated spectra. This demonstrates that the one-dimensional symmetry consideration which holds for confined states actually breaks when the overlap between wave functions of electrons from adjacent wells along the MQW axis starts to play a significant role.

(c) The calculated transitions have an asymmetrical line shape, with sharper edge at higher energies. This intrinsic asymmetry, which is due to the electron mass nonparabolicity (see Fig. 1), is completely washed by the broadening due to the monolayer well width fluctuations. From Fig. 2(b) we thus conclude that the asymmetric spectral shape of the intersubband transitions and their spectral width at low temperatures [Fig. 2(a)] result from monolayer fluctuations in the well width.

(d) In the calculated spectrum shown in Fig. 2(b) (dashed line) we have approximated the integration over $k_{\parallel}$ (along the MQW direction) by an average over the contributions of three equally spaced points within the first MQW BZ. Using five or more $k_{\parallel}$ points yielded identical spectra. In order to learn the relevance of the number of points used for the calculation of the absorption spectrum and the interaction between neighboring wells, we have calculated the absorption due only to the central QW in a nonperiodic structure containing only 3 QWs. The spectrum obtained is strikingly similar to the one shown in Fig. 2(b) (dashed line). This result leads us to believe that the number of points used for the integration over the SL axis indicates the length over which the states maintain their coherence. From agreement between the calculated and the measured spectra, we conclude that electron states in the continuum minibands of this sample must maintain their coherence over distance comparable to at least three MQW periods. This amounts to a few tenths of a micron parallel to the MQW axis. This is possible, since in our InGaAs/InP sample this direction is composed mainly of binary barrier material of good crystallographic quality. Thus, scattering by potential fluctuations is limited in this direction.

In Fig. 2(c) we display the measured absorption spectra of the second sample, in which the separation between adjacent wells is roughly 50% larger than it is in the first one and in which the wells are intentionally n-type doped. The absorption spectrum for light polarized parallel (perpendicular) to the growth direction is given by the solid (dashed) line. For comparison, we also display in Fig. 2(d) the calculated absorption spectra of this sample, for light polarized parallel to the MQW axis. The dashed line in Fig. 2(d) describes the spectrum calculated using [as in Fig. 2(b)] three equally displaced points within the MQW BZ, while the solid line describes the calculations with contribution from the BZ center point only. Clearly, similar to the case of a single QW, mainly the symmetry allowed transitions contribute to the absorption in this case. Comparing the measured and calculated spectra we deduce the following.

(a) Surprisingly, the measured absorption for radiation polarized parallel to the MQW axis (the "allowed" polarization) agrees quite nicely with the spectrum that was calculated using the contribution from the BZ center point only. The spectral positions of the various transitions are adequately given by this calculation. The asymmetric spectral shape of the transitions and their widths are explained as in the previous sample by monolayer fluctuations in the QWs width (not shown). We note that the spectral lines are broader in this sample due to the higher concentration of electrons in its wells. The absolute strength of the $e1$-$e2$ transition agrees with our calculations while the measured transitions to the continuum minibands are a factor of 5 stronger.

(b) The transitions to even continuum minibands in the measured spectrum are stronger than the transitions to odd minibands. We believe that this is a consequence of the phase coherence length of wave functions of carriers in the continuum minibands being comparable to the MQW period length. As a result, wave functions with longer superlattice wavelengths are influenced less by the scattering, maintain their phase coherence, and contribute more to the absorption. The lack of coherence in this sample is due to the larger separation between adjacent QWs, and to the presence of larger concentration of donors and electrons in the QWs.

(c) The calculated spectrum for light polarized parallel to the MQW planes (the "forbidden" direction, not shown) is similar in spectral shape to that shown in Fig. 2(d) by the dashed line. It is, however, weaker by about 3 orders of magnitude. Experimentally, only the transition between the confined subbands $e1$-$e2$ is polarized. The transitions from the confined subband $e1$ to the continuum minibands are only partially polarized. This residual polarization is lost as the order of the transition increases (the same phenomenon was also observed in the first sample). Note also that since in our experiment the radiation propagates at 45° relative to the MQW axis, absorption in the forbidden direction enhances also the measured absorption in the "allowed" direction.

The striking difference between the polarization selection rules of the confined to confined intersubband transition and the confined to minibands transition as observed in both samples was found to be temperature independent

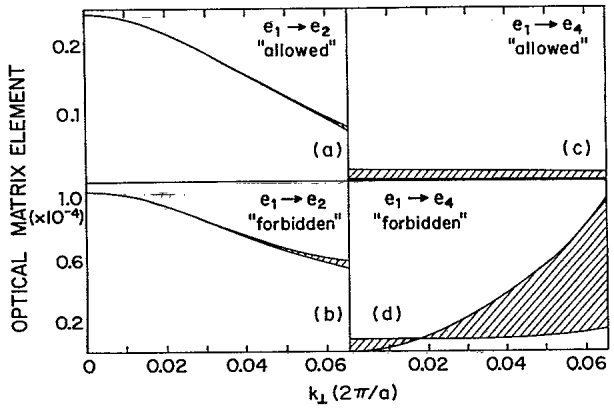

FIG. 3. (a),(b) Optical matrix elements as a function of $k_\perp$, for the $e1$-$e2$ transition for light polarized along the MQW axis and perpendicular to it. (c),(d) Same as (a) and (b) but for the $e1$-$e4$ transition. The optical matrix element is given in units of $E_p m_0/2$, where $E_p = 25.3$ eV [11].

up to room temperature. Though we could not obtain complete quantitative understanding of these polarization selection rules, we believe that some qualitative understanding can be gained by studying the in-plane crystal momentum ($k_\perp$) dependence of the optical matrix elements of the various transitions. In Fig. 3(a) [3(b)] we show the calculated optical matrix elements for the allowed [forbidden] polarization of the $e1$-$e2$ optical transition as a function of $k_\perp$. Similarly, in Fig. 3(c) [3(d)] we show the same for the $e1$-$e4$ optical transition. Other optical transitions from the confined subband $e1$ to the continuum minibands, such as $e1$-$e3$ and $e1$-$e5$, behave qualitatively the same. The calculations relate to the nominal structure of the first sample and the band structure of Fig. 1.

Whereas for all other transitions the optical matrix elements decrease as we move away from the BZ center [Figs. 3(a)–3(c)], the forbidden polarization matrix elements of the confined to expanding optical transition actually *increase* [Fig. 3(d)]. At 10% of the BZ, these forbidden polarization matrix elements increase by almost 2 orders of magnitude from their value in the zone center. We thus attribute the breaking of the polarization selection rule for the confined to expanding optical transitions to in-plane crystal-momentum mixing processes such as scattering and confinement by strong potential fluctuations. These potential fluctuations, which are typical to the doped QW ternary material, affect mainly electron wave functions in directions parallel to the QW planes. Thus, in order to explain our experimental observations more quantitatively, scattering should be included in the multiband theoretical model.

Finally, we have also studied these intersubband transitions by photoinduced absorption. In this technique, the changes in the intersubband absorption as a result of photopopulation of the first conduction subband by above band-gap excitation is measured [15]. The optical transitions from the first subband to the second confined subband and to the minibands within the continuum were clearly observed by this technique as well. Detailed account of this photoinduced intersubband absorption will be reported separately.

In summary, we have studied by means of absorption and photoinduced absorption spectroscopies the optical transitions between confined electronic states of a MQW to minibands in its continuum. By comparison with a theoretical model we spectroscopically identify all the observed transitions and we explain their strength and spectral shape. By comparing the miniband spectrum to that calculated for a finite array of quantum wells, or equivalently to that calculated for a selected number of $k_\parallel$ points, we estimate the coherence length of the wave function of electronic states in these minibands. The newly observed transitions are not polarized parallel to the MQW axis. We qualitatively explain this behavior in terms of the dependence of the optical matrix element of these transitions on the in-plane crystal momentum.

The work at the Technion was carried out in the Center for Advanced Opto-Electronics, and was supported by the Basic Research Foundation Administered by the Israel Academy of Sciences and Humanities, Jerusalem, Israel.

[1] L. C. West and S. J. Eglash, Appl. Phys. Lett. **46**, 1156 (1985).
[2] B. F. Levine, R. J. Malik, J. Walker, K. K. Choi, C. G. Bethea, D. A. Kleinman, and J. M. Vandenberg, Appl. Phys. Lett. **50**, 273 (1987).
[3] A. Seilmeier, H.-J. Hübner, G. Abstreiter, G. Weimann, and W. Schlapp, Phys. Rev. Lett. **59**, 1345 (1987).
[4] P. England, J. R. Hayes, E. Colas, and M. Helm, Phys. Rev. Lett. **63**, 1708 (1989).
[5] H. Asai and Y. Kawamura, Phys. Rev. B **43**, 4748 (1991).
[6] S. D. Gunapala, B. F. Levine, R. A. Logan, T. Tanbun-Ek, and D. A. Humphrey, Appl. Phys. Lett. **57**, 1802 (1990).
[7] F. Capasso, C. Sirtori, J. Faist, D. L. Sivco, S-N. G. Chu, and A. Y. Cho, Nature (London) **358**, 565 (1992).
[8] D. Ritter, R. A. Hamm, M. B. Panish, J. M. Vandenberg, D. Gershoni, S. D. Gunapala, and B. F. Levine, Appl. Phys. Lett. **59**, 552 (1991).
[9] J. M. Vandenberg, D. Gershoni, R. A. Hamm, M. B. Panish, and H. Temkin, J. Appl. Phys. **66**, 3635 (1989).
[10] G. A. Baraff and D. Gershoni, Phys. Rev. B **43**, 4011 (1991).
[11] D. Gershoni, C. H. Henry, and G. A. Baraff, IEEE J. Quantum Electron. (to be published).
[12] W. Zawadzki, J. Phys. C **16**, 229 (1983).
[13] G. Bastard, *Wave Mechanics Applied to Semiconductor Heterostructures* (Les Editions de Physique, Les Ulis, France, 1988).
[14] Y-C. Chang and R. B. James, Phys. Rev. B **39**, 12672 (1989).
[15] J. Oiknine-Schlesinger, E. Ehrenfreund, D. Gershoni, D. Ritter, M. B. Panish, and R. A. Hamm, Appl. Phys. Lett. **59**, 970 (1991).